Polymer 49 (2008) 5458–5466

Contents lists available at ScienceDirect

Polymer

journal homepage: www.elsevier.com/locate/polymer

Investigation of the peel behavior of polyethylene/polybutene-1 peel films using *in situ* peel tests with environmental scanning electron microscopy

Michael Nase [a,b,*], Armin Zankel [c], Beate Langer [b], Hans Joachim Baumann [a], Wolfgang Grellmann [b,d], Peter Poelt [c]

[a] Orbita-Film GmbH, D-06369 Weißandt-Gölzau, Germany
[b] Polymer Service GmbH Merseburg, D-06217 Merseburg, Germany
[c] Institute for Electron Microscopy, Graz University of Technology, A-8010 Graz, Austria
[d] Martin Luther University Halle-Wittenberg, Center of Engineering Sciences, D-06099 Halle/Saale, Germany

ARTICLE INFO

Article history:
Received 2 July 2008
Received in revised form 7 October 2008
Accepted 8 October 2008
Available online 17 October 2008

Keywords:
In situ peel test
ESEM
Peel angle

ABSTRACT

The micro-deformation processes of sealed low-density polyethylene/isotactic polybutene-1 (PE-LD/iPB-1) films with different contents of iPB-1 up to 20 m.-% (mass-percentage) were investigated in this study. The peel process was analyzed in detail using *in situ* peel test measurements with environmental scanning electron microscopy (ESEM). This method enables the direct correlation of recorded force–elongation data with observed structural phenomena. Thus, important parameters, e.g., the peel initiation value, could be determined directly from *in situ* measurements. The dependence of the peel properties on the iPB-1 content was analyzed and the correlation between micro-structure and performance of the peel process was clarified.

Furthermore, the structural reason behind the dependence of the peel properties on the peel angle was identified. The crack propagation types *interlaminar* and *translaminar* were analyzed in detail with the ESEM. The *translaminar* crack propagation was further characterized using a tilted microscope stage with a mounted tensile tester.

The direct contact of the electron beam with the non-conductive sample surface can cause beam damage. The beam damage, indicated by the absorbancy band at 965 cm^{-1} in the infrared spectrum, was investigated in dependence on the total irradiation time.

1. Introduction

Peel systems are often used for packaging to realize an easy-opening of the sealed/closed packages without the use of any cutters or scissors. Such peel systems have more and more a larger part in the packaging industry. For example they were used in the foodstuff sector as well as in the medical sector for protective packages [1,2]. A specific peel system is the combination of low-density polyethylene (PE-LD) with a minor amount of isotactic polybutene-1 (iPB-1), processed to films by blowing process or cast film production [2–9]. The two involved blend parts were incompatible. Thus, they build a matrix–particle structure. In practice, two films were sealed together by application of heat and pressure using a commercial seal device. The easy-opening of such PE-LD/iPB-1 peel films is based on the very low adhesive strength between PE-LD and iPB-1 within the sealed peel film package. Recent investigations on the mechanical behavior of PE-LD/iPB-1 peel films reveal a strong influence of the iPB-1 content on the peel force obtained by T-peel test [7,8]. The peel force is the force, which is necessary to open the sealed peel film. The higher the iPB-1 content, the lower is the peel force. Furthermore, a dependence of the peel properties on the peel angle revealed by fixed arm peel test was pointed out [8]. Two different ranges of the peel angle (between 70° and 120° and between 140° and 180°) connected by a transitional range could be established. Because of the different microscopic appearances of the peel surface (the "fracture" surface of the peeled film), the two zones were referred to as *interlaminar*, i.e., the normal peeling behavior along the center of the seal area, and *translaminar*, i.e., an undefined and/or early separation of the two sealed films.

However the structural reason behind the determined dependencies, mentioned above, is not fully identified up to now. Furthermore, the deformation processes within the seal area need

* Corresponding author. Polymer Service GmbH Merseburg, D-06217 Merseburg, Germany. Tel.: +49 3461 46 2761; fax: +49 3461 46 2592.
E-mail address: michael.nase@psm.uni-halle.de (M. Nase).

0032-3861/$ – see front matter © 2008 Elsevier Ltd. All rights reserved.
doi:10.1016/j.polymer.2008.10.004

to be understood in detail, to establish morphology–property correlations. Therefore, the peel process has to be analyzed in detail by observing the process at different times using scanning electron microscopy (SEM). It is not possible to use the conventional scanning electron microscope for the present investigations, since in this case the samples need to be conductive or have to be covered with a conductive layer. Conductivity of the polymeric peel film can be achieved by, e.g., sputtering the sample surface with gold. However, the conductivity gets lost if the peel process starts. Thus, the environmental scanning electron microscope (ESEM) is a good alternative in comparison to the conventional scanning electron microscope, to observe the peel process [3,10]. The ESEM enables quasi-static and dynamic investigations of non-conducting or wet specimens, because of its specific instrumental setup [10–14]. A tensile test device needs to be applied in the ESEM to investigate the peel process *in situ* at different times. This *in situ* peel test with ESEM can now be used to correlate the observed deformation processes with the force–elongation/peel behavior of the actual peel film sample. A disadvantage of the ESEM is the possibility to cause beam damage, because of the missing conductivity [15,16]. Note that microscopic investigations with conventional scanning electron microscopy also induce beam damage, however, the necessary conductivity of the SEM-samples minimizes the beam damage. In the case of ESEM investigations, the electron beam interacts directly with the sample surface. So, chemical and/or physical destruction of parts of the sample are possible, in dependence on the magnification, the acceleration voltage of the electron beam, the scanning velocity and the total irradiation time of the electron beam on the sample. The beam damage also depends on the material properties, especially on the resistance against heat. So, the beam damage has to be considered for an interpretation of the experimental results.

Summarizing the scope of the present work, it is intended to investigate the proceeding peel process by *in situ* peel test measurements with ESEM. The peel behavior in dependence on the iPB-1 content is investigated to analyze the deformation mechanisms within the seal area. In this context, the peel initiation behavior is analyzed. Furthermore, it is intended to clarify the deformation mechanisms of the *interlaminar* and *translaminar* crack propagations. It is expected that the deformation behavior within the seal area, caused by various peel angles, is strongly different. Finally, the direct correlation of observed deformation processes and recorded force–elongation data enables the determination of quantitative morphology–property correlations. Additionally, the beam damage of the analyzed samples is evaluated, and its influence on the peel behavior is investigated.

2. Experimental

2.1. Materials

Subjects of the investigations were blends of PE-LD and iPB-1 with different mixing ratios (97/3, 94/6, 90/10, 85/15, 80/20). The PE-LD used is Lupolen 2420F with a density of 0.923 g cm^{-3}, and the iPB-1 used is PB 8640M, acting as minor blend component, both provided by LyondellBasell (Germany). The melt-flow index of PE-LD, determined at 503 K with a load of 2.16 kg, is 0.73 g (10 min^{-1}). Furthermore, the melting temperature of the PE-LD used is about 384 K, and the crystallinity is about 38%. The iPB-1 of the present study is a statistical copolymer with low amount of ethylene, and the melt-flow index, determined at 503 K with a load of 2.16 kg, is 1 g (10 min^{-1}). The melting temperature of iPB-1 is about 386 K, and the crystallinity is about 40% and therefore similar to PE-LD. The polymer blends were processed to films by blowing process (lab equipment) at Orbita-Film GmbH (Germany) using a set of standard processing conditions (Table 1).

Table 1
Processing conditions of the peel film production.

	Processing conditions	Standard values
Extruder	Mix and shear element	With maddock mix and shear element
	Screw speed	100 min^{-1}
	Temperatures of the extruder zones	140–160–180–180–180 °C
Die head	Temperatures of the die head zones	180–180–180–180 °C
	Die gap size	0.8 mm
Tube forming area	Time of solidification	1.8 s
	Blow-up ratio	1:2
	Draw-down ratio	1:7.85

After film production, the peel test samples were prepared. Therefore, the films were sealed at a temperature of 140 °C, for a period of time of 2 s, and, subsequently, the sealed films were cooled to ambient temperature.

2.2. Instrumentation

2.2.1. Microscopy

The *in situ* investigations were performed in an ESEM Quanta 600 FEG from FEI (Eindhoven, The Netherlands), working in the low vacuum mode (nominally about 0.1–2.5 torr) [13]. The specific imaging principle of the ESEM, which enables the investigation of non-conducting specimens, is described elsewhere [11,12,14]. In the present study, the high voltage was 10.0 kV, the probe current was 0.4 nA, the pressure of the imaging gas (water vapour) was 66.7 Pa, and the working distance was about 11.3 mm.

2.2.2. In situ *T-peel test*

The *in situ* T-peel test was applied for simultaneous structural and mechanical investigations of the proceeding peel process at ambient temperature. The performance of the *in situ* T-peel test is similar to the performance of the T-peel test outside the ESEM [8,17–19]. A micro-deformation device (MT5000 from Deben; Suffolk, UK), which was mounted in the sample chamber, was used for this *in situ* peel test. The micro-deformation device and, even more, the peel film samples were placed in the sample chamber in such a manner that an observation of the peeling seal area is possible (Fig. 1). Therefore, the micro-deformation device draws the peel film symmetrically. The initial distance between the clamps was 42.5 mm, and the peel rate was 1 mm/min. The simultaneous record of the ESEM images and the mechanical data (force–elongation data, peel curve) enables the direct determination of the peel initiation behavior of the peel films. Therefore, it is determined the force F_i, at which the first local peeling could be observed by ESEM. The peel behavior in dependence on the iPB-1 content was quantified by calculating the energy release rate G_{Ic}, which is given by Eq. (1) and further described in a separate study [8]. E_G is the total peel energy, which corresponds to the area under the force–elongation diagram (peel curve), W is the width of the seal area, and L is the length of the seal area.

$$G_{Ic} = \frac{E_G}{WL} \tag{1}$$

2.2.3. In situ *fixed arm peel test*

The *in situ* fixed arm peel test could not be directly performed, because of the missing micro-deformation device with an adjustable wide range of the peel angles. Nevertheless, two extreme peel angles (90° and 180°) were realized by modifying the test assembly, to perform a peel test measure of each crack propagation zone (*interlaminar* and *translaminar*) at ambient temperature.

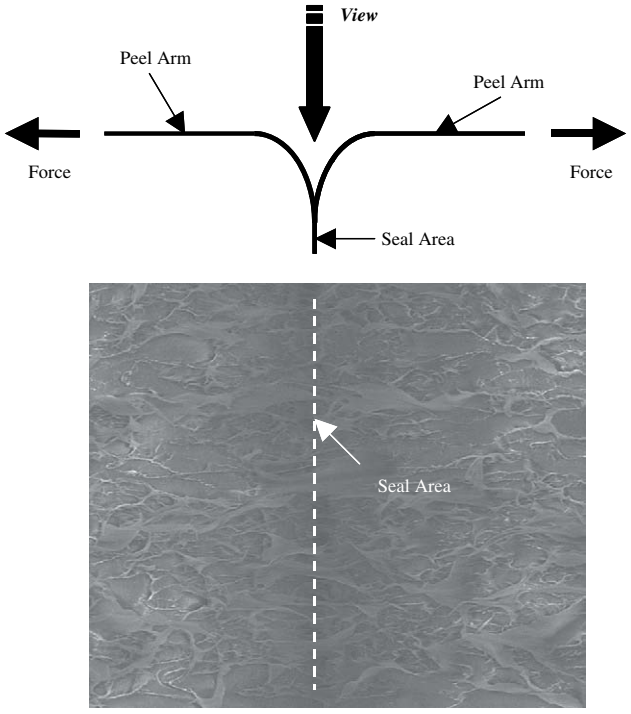

Fig. 1. Schematic of the observation process of the peel film samples within the ESEM sample chamber. A direct view into the peeling seal area is realized.

A T-profile with a peel film sample attached on the front side was used to realize 90° peel angle, and an I-profile with a peel film sample attached on the surface was used to realize 180° peel angle (Fig. 2). The initial distance between the clamp and the coated part of the film on the I- or T-profile was 25 mm, and the peel rate was 1 mm/min.

2.2.4. Fourier transformed infrared (FTIR) spectroscopy

The influence of beam damage was investigated using FTIR. An IR spectrometer (Bruker Equinox 55) with attenuated total reflection (ATR) setup was used.

3. Results and discussion

3.1. Investigation of the proceeding peel process

The peel curve progression of the proceeding peel process exhibits several points of interest, which were analyzed in detail by observing the process at different times using *in situ* T-peel test with ESEM. This investigation helps to understand the micro-deformation processes during peeling, caused by mechanical loading. Fig. 3a shows an exemplary peel curve, force as a function of elongation, of the blend PE-LD/iPB-1 with 10 m.-% iPB-1. The raw-data show two local maxima, which were addressed to the geometry of the peel film sample. The partially molten polymer moves to the border of the sample due to the inserted pressure of the two seal plungers of the seal device, during sealing at 140 °C. Thus, the cross-section of the seal area became a concave appearance. This phenomenon leads to the increased force in the boarder of the seal area. The plateau-like curve progression between the two local maxima was used to calculate the peel force (between 20% and 80% of the elongation at break) [8], i.e., the average force in this curve-range. The peel force is about 1.15 N, of the present PE-LD/iPB-1 blend with 10 m.-% iPB-1. The peel curve exhibits eight points of interest, whose corresponding ESEM images are shown in Fig. 3b–i. These eight points of interest of the peel curve progression will now be analyzed in detail. At the beginning of the peel process, the seal area, which runs vertical relating to the image width, is fully closed (Fig. 3b). The seal area is locally open after about 0.7–0.9 mm elongation. This phenomenon is called "peel initiation" according to the "crack initiation" behavior, which is often used in fracture mechanics investigations of materials [20–23]. The crack initiation is at the beginning of the stable crack growth, which generally occurred before the unstable crack growth, and is hereinafter called "peel initiation" because of the use outside the usual fracture mechanics concepts. This peel initiation can be seen in Fig. 3c. The peel initiation is a local phenomenon, because of the non-linear border of the seal area, caused, among others, by the unbalanced thermal radiation during sealing. The corresponding force to the observed first local peeling in the force–elongation diagram (cf. Fig. 3a) is hereinafter called "peel initiation force" F_i and indicates the local beginning of the peel process. The peel initiation force is actually about 0.2 N. The slope of the peel curve changes after about 1.5 mm elongation (marked by the dotted lines). The change of the slope corresponds with the formation of the crack front (peel beginning, concerning the total length of the seal area), which is shown in Fig. 3d. Some vertical structured domains are shown within the deformation areas of the seal area (marked by an arrow in Fig. 3d). These domains result from the distortion of microscopic parts of the peel film as a consequence of the thermal radiation during sealing. The peel process shows a continuous progression (Fig. 3e) at the beginning of the peel curve plateau at 20% of the elongation at break. Plastic deformations could be observed and there is a high degree of structuring within the seal area. Note that it is not possible to separate visually the matrix PE-LD and the peel component iPB-1 by ESEM. There is no material specific contrast like in a transmission electron microscope (TEM), since the material is not differentially

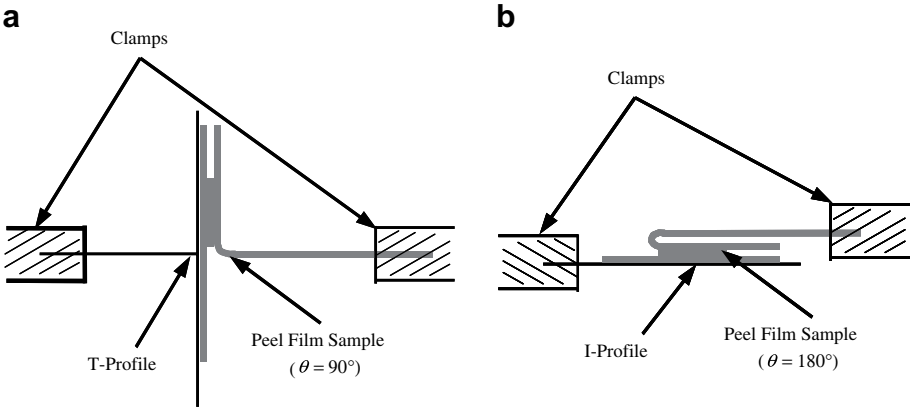

Fig. 2. Schematic of the fixed arm peel test arrangements for a peel angle $\theta = 90°$ (a), and $\theta = 180°$ (b).

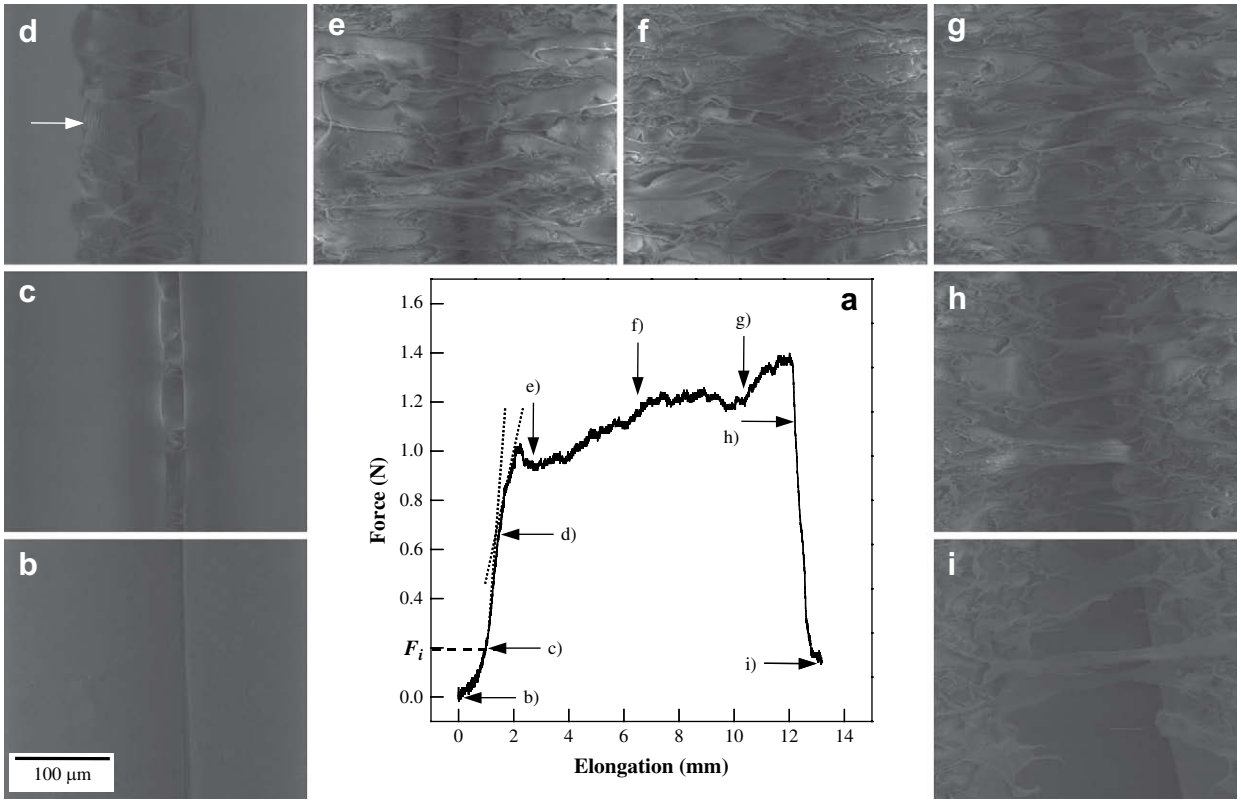

Fig. 3. Force–elongation diagram (peel curve) of PE-LD with 10 m.-% iPB-1 (a) and the corresponding ESEM images at different positions of the peel process (b–i), obtained by *in situ* T-peel test with ESEM. The scaling-bar of Fig. 3b is also used for c–i.

stained [24,25]. However, the ESEM images enable to comprehend the peel process, and to understand the peel behavior in more detail at microscopic scale. The similarity of the deformation areas at the beginning (Fig. 3e), in the middle (f) and at the end (g) of the plateau-like curve progression evidences a continuous and defined crack propagation through the seal area of the two peel films. There is a steep front of the load subsequently to the second local maximum. It starts with the decomposition of the crack front at about 12.5 mm elongation, which is monitored in Fig. 3h. The existence of a decomposition process of the crack front reveals a slightly unequal crack front, similar to the case of crack front formation at the beginning of the peel process. The decomposition process of the crack front can

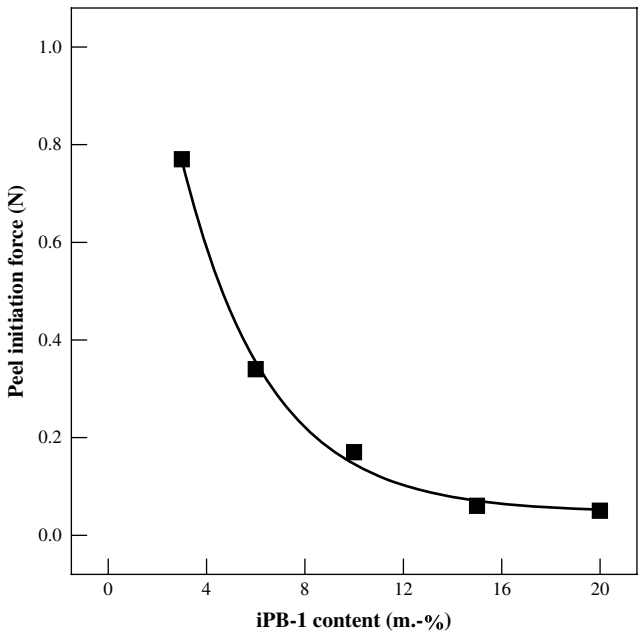

Fig. 4. Peel initiation force F_i as a function of iPB-1 content, obtained by *in situ* T-peel test with ESEM.

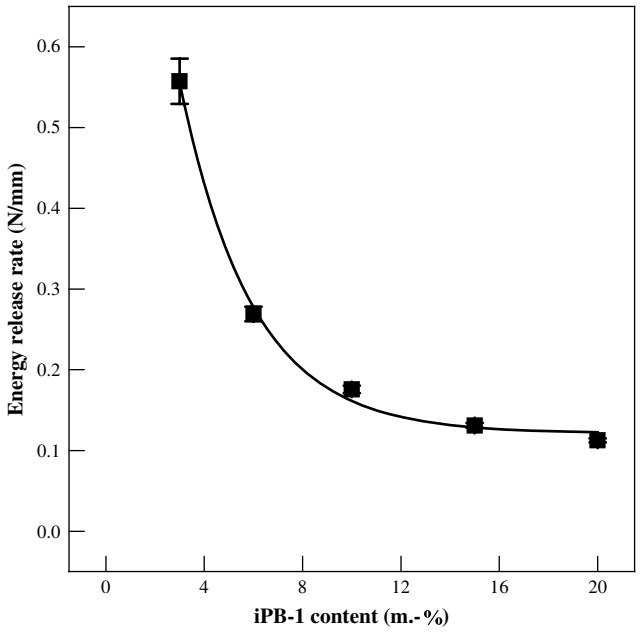

Fig. 5. Energy release rate G_{Ic} as a function of iPB-1 content, obtained by *in situ* T-peel test. The solid line was achieved by fitting the experimental data using an exponential function.

also be due to different local peel rates within the seal area. However, the slightly unequal crack front as a result of inhomogeneous thermal radiation during sealing is favored as the major cause for this process. The complete separation of the two sealed films is observed after about 13 mm elongation, which is shown in Fig. 3i. The *in situ* peel test investigation reveals that the peel process is very complex. However, the process can be observed in detail at microscopic scale by ESEM. Furthermore, the peel process can be equated with a stable crack growth process, because of the necessity of an energy input to realize the proceeding peeling. If the energy input stops (in this case the mechanical loading), the peel process also stops.

3.2. Investigation of the influence of iPB-1 content on peel properties

Another aim of this study was the identification of the micro-deformation processes within the seal area for peel films with different contents of iPB-1. The iPB-1 content influences directly

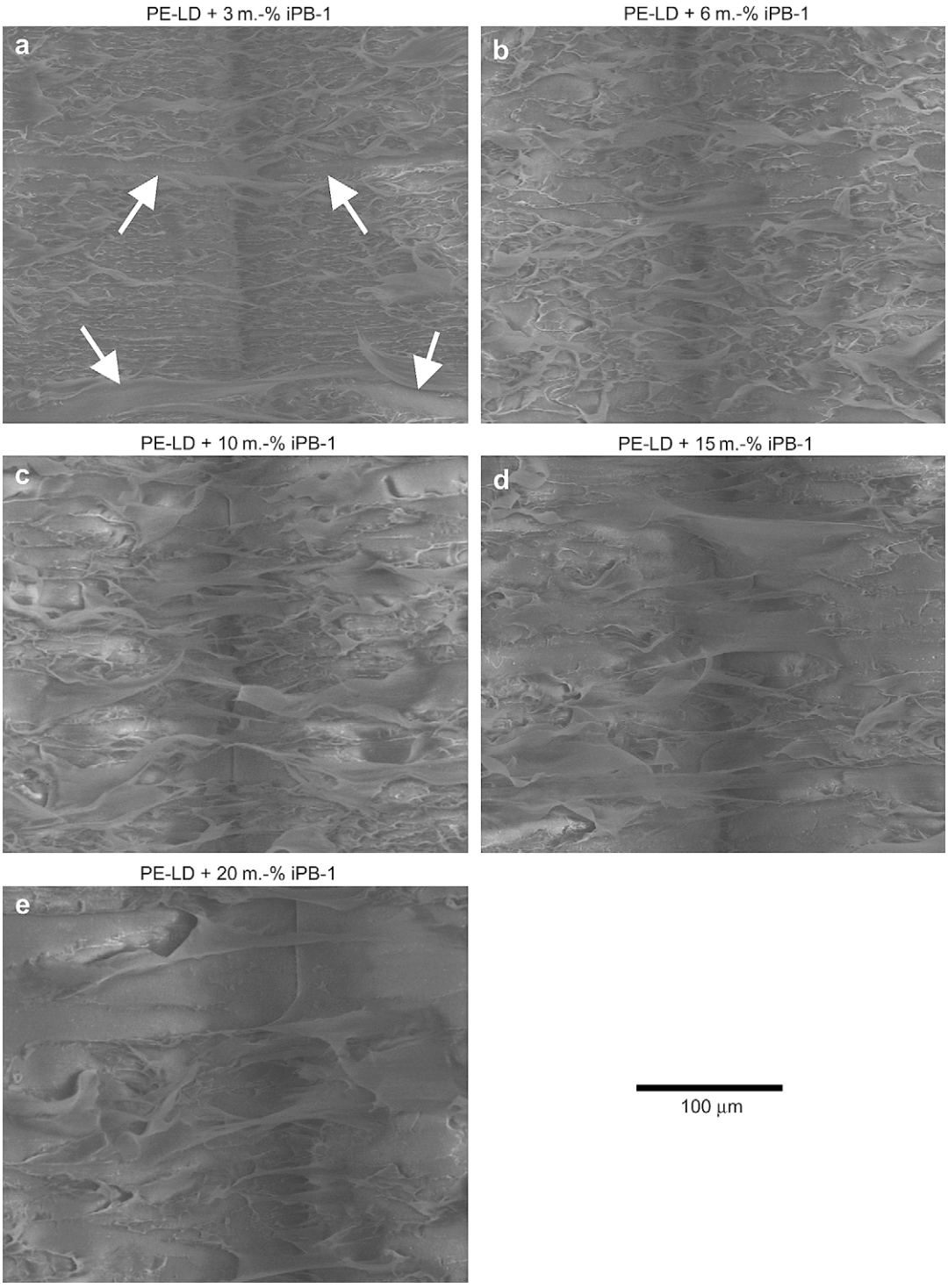

Fig. 6. ESEM images of PE-LD with 3, 6, 10, 15, 20 m.-% iPB-1, corresponding to the determined data of Fig. 4. The images were taken at about 50% elongation. The white arrows denote some imperfections within the seal area during peeling.

the peel properties as already pointed out in different studies [5,8]. At first, the peel initiation behavior was analyzed. The investigation of the peel initiation behavior is of scientific and practical interest, among the analyses of the occurred micro-deformation processes within the seal area. Fig. 4 is a plot of the peel initiation force F_i as a function of iPB-1 content. The data reveal an exponential decrease by about 90% of the peel initiation force in dependence on the iPB-1 content, with a reciprocal decay constant of 3.5 m.-%. In a further step, the peel behavior was quantified using the energy release rate. Fig. 5 shows the energy release rate G_{Ic} as a function of iPB-1 content, obtained by *in situ* T-peel test. Their dependence on the content of iPB-1 is of exponential character, with a reciprocal decay constant of 3.0 m.-%. The energy release rate decreases with increasing iPB-1 content by about 80%, and therefore shows a slightly smaller decrease than the peel initiation force (cf. Fig. 4). The corresponding ESEM images to the energy release rate–iPB-1 content data of Fig. 5 are shown in Fig. 6a–e, and were taken when the peel process reached the middle of the plateau-like curve progression at about 50% elongation. The images clearly show the deformation mechanisms during the peel process. There are fibrillic structures, which connect the currently opened parts of the seal area. These fibrillic structures result from a stretching of parts of the film-material within the seal area in direction of both load-application points. The elongated parts can be PE-LD as well as PE-LD with iPB-1. The elongated parts were originally surrounded and/or penetrated by numbers of predetermined breaking points, i.e., the interface between PE-LD and iPB-1. An agglomeration and/or favorable arrangement of such predetermined breaking points result in a defined damage zone, which is used as favorable path of the crack. The number of breaking points, which are able to agglomerate, increases with increasing iPB-1 content, and therefore the number is the lowest for PE-LD with 3 m.-% iPB-1 (Fig. 6a). However, the numbers of fibrillic structures decrease with increasing iPB-1 content. Thus, the number of possible fibrillic structures is the highest for PE-LD with 3 m.-% iPB-1. Furthermore, imperfections are shown in the peeled seal area only for PE-LD with 3 m.-% iPB-1. The imperfections were marked by white arrows (cf. Fig. 6a). Such imperfect parts of the seal area during the peel process were not observed for iPB-1 contents $\geq$6 m.-%, which can be due to an inhomogeneous arrangement of the iPB-1 domains within the seal area. So, the ESEM result is in agreement with the result of the TEM measurements, which were published elsewhere [3,7]. The TEM investigations reveal a stable and reproducible peel process only for iPB-1 contents $\geq$6 m.-%, as a result of the continuous belt-like alignment of the iPB-1 domains within the seal area. Additionally, the ESEM images of Fig. 6 also show an increase of the dimension of the fibrillic structures with increasing content of iPB-1. This fact is not contradictory to the decreased peel force for enhanced mass fraction of iPB-1. The iPB-1 domains are highly aggregated especially for PE-LD with 20 m.-% iPB-1. So, the number of possible fibrillic structures is reduced. Note that not only the domains of iPB-1 are aggregated and consequently enlarged, but also the iPB-1 content within the fibrillic structures is increased, as a result of enhanced mass fraction of iPB-1. Thus, these fibrillic structures with a large content of iPB-1 can be more elongated than those with a minor content of iPB-1. These were the reasons why the dimension of the fibrillic structures seems to be enlarged with increasing iPB-1 content. Fig. 6e also partially shows the absence of deformation areas within the seal area as a consequence of the aggregated iPB-1 domains and minor numbers of fibrillic structures.

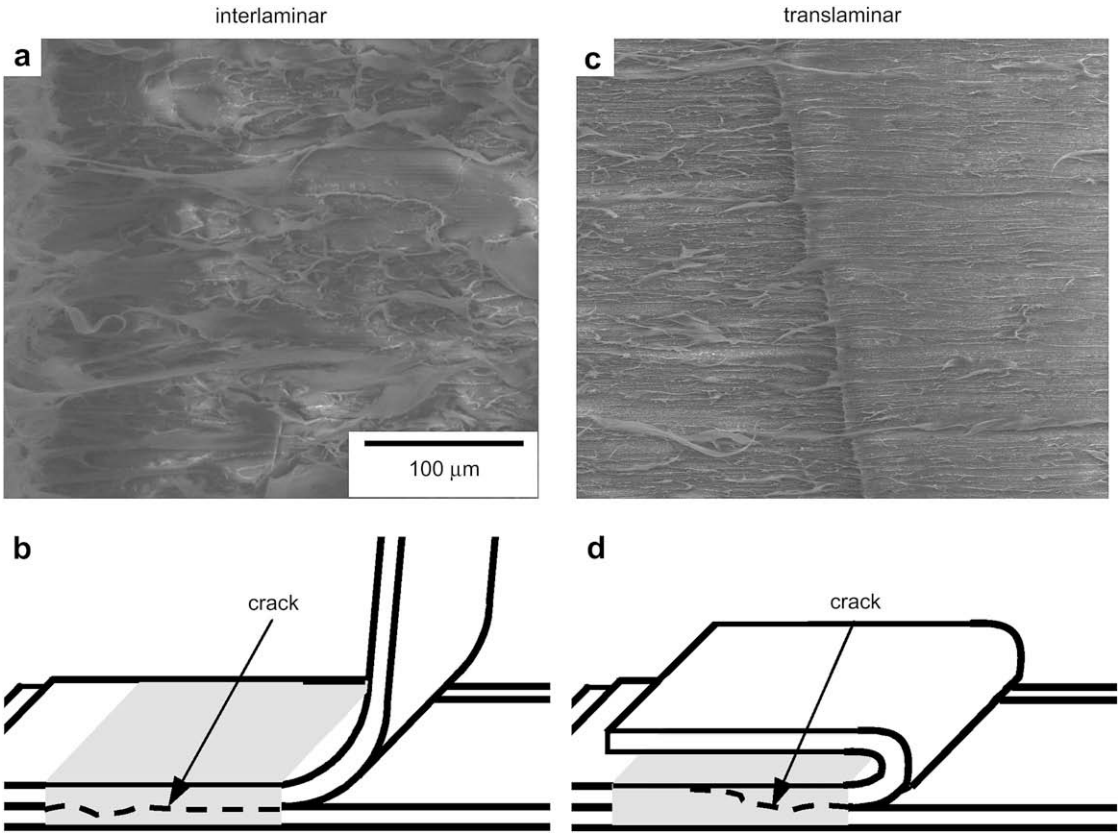

Fig. 7. ESEM image of the *interlaminar* crack propagation (a) and the corresponding schematic (b), as well as the ESEM image of the *translaminar* crack propagation (c) and its corresponding schematic (d). The dashed lines represent the course of the crack.

The *in situ* peel test investigations with ESEM enabled a profound analysis of the deformation processes within the seal area in dependence of the content of iPB-1.

3.3. Investigation of the influence of the peel angle on the peel properties

Now, the ESEM is used to identify the structural reason behind the dependence of the peel properties on the peel angle by *in situ* measurements. The existence of two zones of different crack propagations can be verified by *in situ* peel test measurements with ESEM. The ESEM images of one representative peel film sample of each crack propagation zone (90° *interlaminar*, 180° *translaminar*) are shown in Fig. 7, for PE-LD with 10 m.-% iPB-1. The ESEM images were taken at about 50% elongation. The *interlaminar* peel process is visualized in Fig. 7a and b. The ESEM image shows moderate plastic deformations and a balanced degree of structuring with no imperfections within the seal area and, consequently, a stable and reproducible peel process occurs. Thus, the crack grows along the center of the seal area, which is schematized in Fig. 7b, for *interlaminar* crack propagation using a selected peel angle of 90°. In contrast to this, the ESEM image of Fig. 7c shows more elongated fibrillic structures, which reveal a much higher adhesive energy input. Another difference to the *interlaminar* peel process of Fig. 7a is the existence of a tilted crack front, that points out different peel rates and/or different degrees of deformation of the seal area as a consequence of different courses of the crack. So, a *translaminar* crack propagation occurs for a selected peel angle of 180°. This means, the crack grows over the cross-section of the film in an undefined manner, so that this can lead to an early separation of the two sealed peel films, as monitored in Fig. 7d. The two crack propagation phenomena (two strongly different courses of the crack) *interlaminar* and *translaminar* could be verified using the representative peel angles 90° and 180°. Because of the clear separation of the two crack propagation zones by fracture mechanics analysis [8], it can be stated that the type of crack propagation is identical in the complete crack propagation zone. Thus the crack propagation is *interlaminar* in the range of peel angle of 70° up to 120°, and is *translaminar* in the range of 140° up to 180°.

The *translaminar* peel process needs to be avoided in practice. Therefore, an investigation of the *translaminar* peel process in more detail proves as useful. Fig. 8a–d shows the *translaminar* crack propagation of the peel film sample PE-LD with 10 m.-% iPB-1 for a peel angle of 180°. Fig. 8a shows clearly the right peel arm with the thickness d_{F1} and the crack/peel front, marked by the white, dashed line. Furthermore, a local peel initiation is observed. Typical *interlaminar* deformation areas and a balanced degree of structuring are shown in Fig. 8b, after about 3 mm elongation. A transition from *interlaminar* to *translaminar* crack propagation can be observed in Fig. 8c after about 9 mm elongation, since the

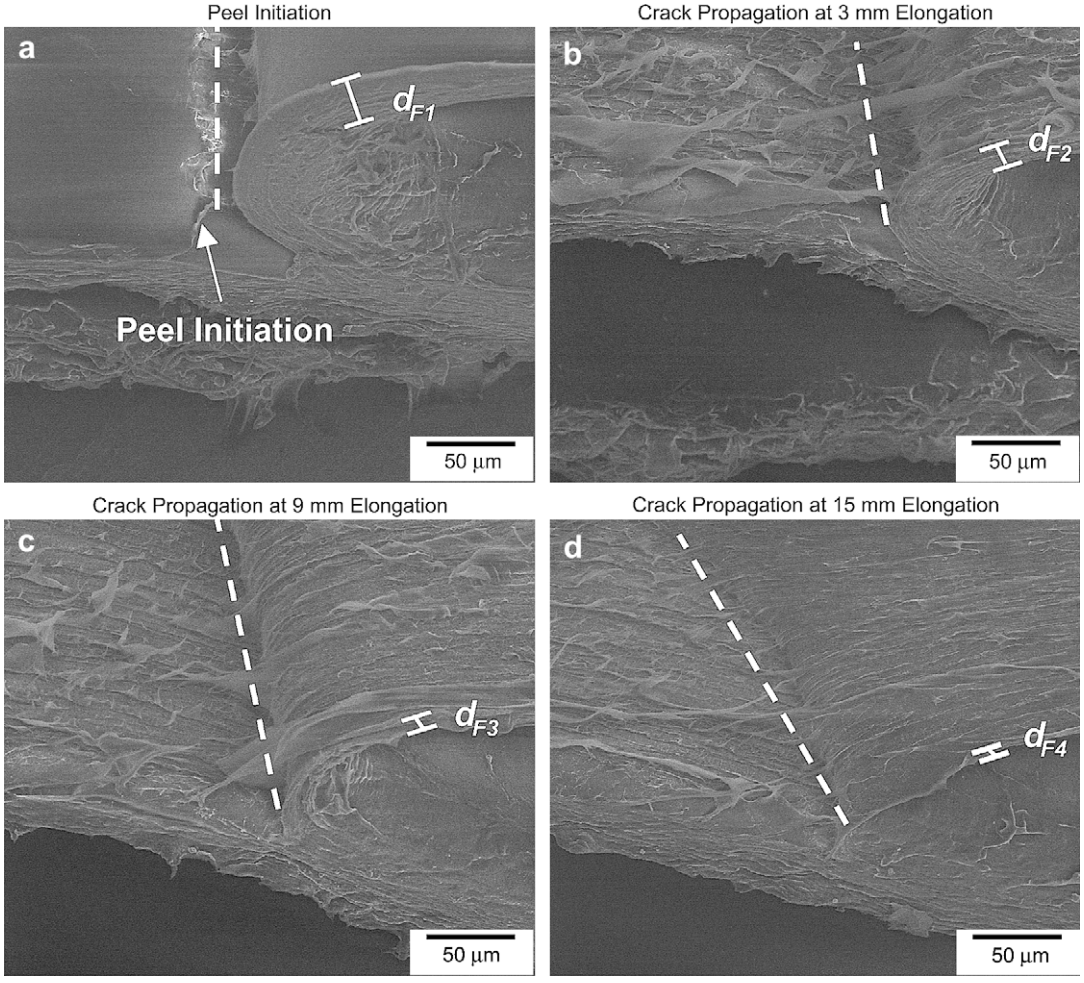

Fig. 8. *Translaminar* crack propagation of the peel film sample PE-LD with 10 m.-% iPB-1 for a peel angle of 180° at different times of the peel process, obtained by *in situ* fixed arm peel test measurements with ESEM (tilted view). The different thicknesses of the peel arm were indicated by d_{F1}, d_{F2}, d_{F3}, and d_{F4}, at nearly 0, 3, 9 and 15 mm elongation, respectively.

fibrillic structures are more elongated and the thickness d_{F3} of the peel arm is smaller than d_{F1} and d_{F2}. The trend continues for 15 mm elongation (Fig. 8d). A strongly tilted crack front could be observed in addition to the distinctly elongated fibrillic structures as a characteristic of the *translaminar* crack propagation. Furthermore, the thickness of the peel arm d_{F4} is the smallest. This fact evidences a *translaminar* course of the crack over the cross-section of the film. The seal area of Fig. 8d is near the total separation of the sealed peel films. It can be stated that a peel angle of more than 140° leads to a *translaminar* course of the crack, which causes undefined and uncontrolled separation of the two sealed peel films. The detailed investigation of the *translaminar* peel process reveals that an *interlaminar* crack propagation occurs first, which converts in a *translaminar* crack propagation after a specific period of time.

It is further assumed that the mentioned transition from *interlaminar* to *translaminar* crack propagation within the *translaminar* crack propagation zone depends on the content of iPB-1 as well as on the peel angle.

3.4. Investigation of the influence of beam damage on the peel properties

The electron beam interacts directly with the sample surface in the environmental scanning electron microscope. Thus, physical and/or chemical damaging of the sample as a consequence of the direct contact with the electron beam cannot be excluded [15,26,27]. Therefore, an investigation of the possible occurring beam damage proves as useful for an accurate evaluation of the determined *in situ* peel test results. The amount of beam damage in polymers depends on the electron dose, which is determined by the probe current, the irradiation time (including also scanning velocity), the irradiated area (including also magnification of the observation) and the type of imaging gas used in the ESEM. A complete analysis of these influences on the beam damage is part of a separate study [16]. Only the magnification of the observation and the total irradiation time of the electron beam were varied in the present study. So a large magnification (field width of the irradiated area: 320 μm) was chosen for the beam damage analysis in dependence on the total irradiation time of the beam. *In situ* investigations reveal that obvious structures need about 25 s to move out of the sphere of influence of the electron beam. Thus, a period of time of 30 s is considered as an upper limit for the irradiation time during the present experimental investigations. Now, identical samples were irradiated for different periods of time and investigated using the FTIR spectroscopy. Fig. 9 shows four Infrared spectra, recorded after different irradiation times. The IR-absorbancy band at 965 cm^{-1} shows some remarkable and the absorbancy band at 908 cm^{-1} shows some minor differences in dependence on the total irradiation time of the electron beam. The absorbancy band at 965 cm^{-1} corresponds to the incidence of alkene *trans* double bonds, and the absorbancy band at 908 cm^{-1} indicates the existence of vinyl end groups. The detected double bonds (band at 965 cm^{-1}) can occur due to (1) separation of nearby hydrogen atoms from the polymer chain and/or (2) formation of vinyl end groups as a consequence of chain-splitting and transfer of radicals. The formation of vinyl end groups is favored as the major cause for the formation of double bonds, since the increase of the absorbancy band at 908 cm^{-1} with increasing irradiation time evidences this fact, and a separation of two nearby hydrogen atoms proves as minor supposable. Nevertheless, the absorbance at 965 cm^{-1} indicates the amount of beam damage for the investigated film. The absorbance increases with increasing irradiation time. The beam damage has the highest values for 600 s and 1800 s irradiation times. The absorbance shows no significant increase for 30 s irradiation time. In other words, the electron beam does not significantly influence the properties of the peel film samples in the present investigations, since the irradiation time is less than 30 s. However, the influence of beam damage needs to be considered especially for static ESEM measurements of polymer samples.

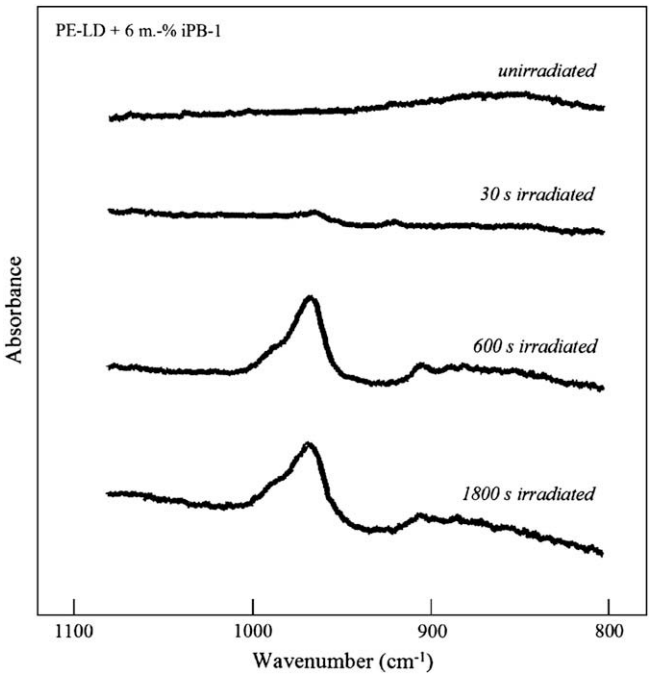

Fig. 9. Infrared spectra of PE-LD with 6 m.-% iPB-1 recorded after different irradiation times.

4. Conclusions

The *in situ* peel test investigations with ESEM of sealed PE-LD/iPB-1 films with different contents of iPB-1 were reported in this study.

The proceeding peel process was investigated in detail by observing the process at different times using *in situ* T-peel test with ESEM. The investigation reveals that the peel process can be equated with a stable crack growth process.

The analysis of the peel initiation behavior shows a decrease of the peel initiation force by about 90% with increasing iPB-1 content. The *in situ* investigations in dependence on the iPB-1 content reveal a stable and reproducible peel process, i.e., the peeled seal area is free of imperfections, only for iPB-1 contents ≥6 m.-%.

The *in situ* investigations with ESEM of the dependence of the peel properties on the peel angle confirm the existence of the two characteristic crack propagation zones *interlaminar*, i.e., the crack grows along the center of the seal area, and *translaminar*, i.e., the crack grows over the cross-section of the film. The strongly elongated fibrillic structures and the tilted crack front, respectively, are characteristics of the *translaminar* crack propagation, which needs to be avoided in practice. Furthermore, it can be stated that also in case of *translaminar* crack propagation an *interlaminar* crack propagation occurs first.

The results of the investigation of the influence of beam damage point out that the actual beam damage is insignificant and can be disregarded for the maximum irradiation time of less than 30 s in the ESEM.

Acknowledgments

The authors gratefully acknowledge financial support by the European Regional Development Fund (ERDF), and by the federal

state Saxony-Anhalt (Germany). Furthermore, the authors thank Dr. Boril Chernev (Institute for Electron Microscopy, Graz University of Technology, Graz, Austria) for providing the FTIR spectroscopy investigations.

References

[1] Stober P, Rist H. Kunststoffe 2004;6:66–9.
[2] Hwo CC. J Plast Film Sheeting 1987;3:245–60.
[3] Nase M, Zankel A, Langer B, Baumann HJ, Grellmann W. In: Proceedings of international conference scanning 2007, Monterey, USA; 2007. p. 50–1.
[4] Geißler G, Kaliske M, Grellmann W, Nase M. Eng Comp 2007;24:586–607 (winner of the outstanding paper award of the Emerald Literati Network).
[5] Nase M, Langer B, Baumann HJ, Grellmann W. In: Proceedings of International Conference "Deformation and Fracture Behavior of Polymers", Merseburg, Germany; 2007. p. 283–311.
[6] Nase M, Androsch R, Langer B, Baumann HJ, Grellmann W. J Appl Polym Sci 2008;107:3111–8.
[7] Nase M, Langer B, Baumann HJ, Grellmann W, Geißler G, Kaliske M. J Appl Polym Sci, in press.
[8] Grellmann W, Langer B, Nase M, Baumann HJ. In: Proceedings of International Conference "Werkstoffprüfung", Bad Neuenahr, Germany; 2006. p. 439–44.
[9] Roucourt I. In: Proceedings of International Conference "Dubai Plast Pro 2007", Dubai, Vereinigte Arabische Emirate; 2007.
[10] Zankel A, Poelt P, Gahleitner M, Ingolic E, Grein C. Scanning 2007;29:261–9.
[11] Hopfe J, Füting M, Wagner S, Pippel E, Woltersdorf J, Hähnel A. Electron Microsc Imaging Anal Surf 1993;26:31–40.
[12] Michler GH, Lebek W. Ultramikrotomie. München: Carl Hanser Verlag; 2004.
[13] Stokes DJ. Technol Edu Microsc 2006:564–70.
[14] Rattenberger J. Advanced investigations of electron–gas interaction in an ESEM used for contrast formation. Master thesis, Graz University of Technology, Graz, Austria: Academic Press; 2006.
[15] Egerton RF, Li P, Malac M. Micron 2004;35:399–409.
[16] Zankel A, Chernev B, Poelt P, Wilhelm P, Nase M, Langer B, et al. Macromol Symp 2008;256:156–65.
[17] ASTM D 1876: Standard test method for peel resistance of adhesives (T-peel test); 2001.
[18] Kinloch AJ, Lau CC, Williams JG. Int J Fract 1994;66:45–70.
[19] Williams JA, Kauzlarich JJ. Tribol Int 2005;38:951–8.
[20] Grellmann W, Seidler S, Jung K, Kotter I. J Appl Polym Sci 2001;79:2317–25.
[21] Starke JU, Michler GH, Grellmann W, Seidler S, Gahleitner M, Fiebig J, et al. Polymer 1998;39(1):75–82.
[22] Grellmann W, Seidler S, editors. Deformation and fracture behaviour of polymers. New York: Springer-Verlag; 2001 [chapter 1].
[23] Anderson TL, editor. Fracture mechanics. Taylor & Francis; 2005.
[24] Goldstein JI, Newbury DE, Echlin P, Joy DC, Lyman CE, Lifshin E, et al. Scanning electron microscopy and X-ray microanalysis. 3rd ed. New York: Kluwer Academic/Plenum Publishers; 2003.
[25] Sawyer LC, Grubb DT. Polymer microscopy. 2nd ed. Chapman and Hall; 1996.
[26] Kitching S, Donald AM. J Microsc 1998;190:357–65.
[27] Hainsworth SV. Polym Test 2006;26:60–70.